Efficient RF Circuit Simulation Using an Innovative Mixed Time-Frequency Method

Jorge F. Oliveira and José C. Pedro, *Fellow, IEEE*

***Abstract*—This paper suggests an answer to the problem of simulating heterogeneous wireless systems composed of baseband and RF blocks, as the former demand for SPICE-like engines, while the latter are more efficiently solved with frequency-domain tools as harmonic balance. The proposed time-frequency hybrid technique splits the circuit's node voltages or mesh currents into fast and slowly varying state variables treating the former with the popular envelope transient harmonic balance technique and the latter with a pure time-marching engine. This way, the circuit's hardest nonlinearities—and their rich harmonic content responses—are appropriately computed in the natural time domain, while the more moderate ones—and their corresponding smooth narrowband RF modulated signals—are efficiently processed in the frequency domain. Simulation tests performed in two illustrative application examples, revealed evident gains in computation speed over state-of-the-art RF simulation tools without any noticeable loss in accuracy.**

***Index Terms*—Circuit simulation, computer-aided analysis, time-frequency analysis.**

I. Introduction

CURRENTLY, there is a strong need for integrated and reconfigurable wireless systems, a goal that is being pursued recurring to the extensive use of baseband processing units, mostly in the digital domain—for control and signal processing—but also, although to a less extent, in analog form—for signal conditioning. Thus, future wireless RF integrated circuits (RFICs), or even systems-on-a-chip (SoCs), devices will tend to be composed of a large set of baseband circuits, plus some smaller front end blocks especially designed for achieving the necessary wireless spectrum confinement, signal dynamic range, and power efficiency.

Typical baseband analog and digital integrated circuits involve a large number of strongly nonlinear components plus a reduced set of linear reactive components because the latter usually present a low quality factor and occupy a very large chip area. In addition, they are supposed to deal with aperiodic low-pass/low-frequency broadband signals presenting abrupt transitions (i.e., showing a rich harmonic content). They are, therefore, naturally amenable to be simulated using SPICE-like engines.

On the other hand, integrated, but mostly hybrid, RF/microwave circuits involve a comparatively larger number of linear reactive components than nonlinear ones, and are designed to deal with either periodic high-frequency carriers or narrowband band-pass/high-frequency modulated signals. Furthermore, due to the frequencies involved, the lumped approximation of most of the reactive component models is no longer valid, and some of them are even naturally described in the frequency domain. Therefore, these RF blocks are more efficiently simulated in frequency domain, using harmonic balance (HB), or in a time-frequency domain, using the envelope transient harmonic balance (ETHB) [1]–[4].

Due to this circuit's heterogeneity, the wireless circuit designers have to rely on a simplified system-level description (circuit-level/system-level co-simulation methodology) in which critical parts of the system are simulated at the circuit level, while most of the remaining blocks are represented with a simplified, many times inaccurate, system-level description.

Unfortunately, this system-level methodology presumes the various circuit blocks do not interact. When this assumption is exposed, for example, because some baseband and RF subcircuits are intricately mixed, the designer must build lumped models for each of the distributed elements and then rely on full circuit-level simulation, usually with a highly inefficient time-marching engine such as SPICE.

In fact, what designers would like to have at their disposal is the best of the two simulation worlds: a SPICE-like simulation tool for the baseband (analog and digital) blocks and HB, or ETHB, for the RF blocks. This work suggests an answer to this ambition detailing and explaining the innovative solution to this problem previously advanced in [5].

The numerical technique now described is supported on the previous ideas of Asai and Makino [6], [7] and on a recently proposed variation of the ETHB technique by Rizzoli *et al.* [8], which consists of using conventional HB or ETHB with a different number of harmonics for variables in different parts of the circuit according to their degrees of smoothness. In this work, we take this idea to its extreme treating some of the state variables with only the zero harmonic component, i.e., exclusively in the time domain. Moreover, we will consider an alternative version of ETHB [9] that we will denote as multitime ETHB, which is based on a multivariate partial differential equation formulation [10], [11]. Despite presenting similar efficiencies,

Manuscript received October 27, 2010; accepted November 09, 2010. Date of publication December 17, 2010; date of current version April 08, 2011. This work was supported in part under Project PTDC/EEA-TEL/65988/2006 Digital_PAs and Project SWIPA P423. The work of J. F. Oliveira was supported in part by the Portuguese Foundation for Science and Technology (FCT) under a Ph.D. grant.

J. F. Oliveira is with the Electrical Engineering Department, Polytechnic Institute of Leiria, 2411-901 Leiria, Portugal (e-mail: jorge.oliveira@ipleiria.pt).

J. C. Pedro is with the Department of Electronics, Telecommunications, and Informatics, Instituto de Telecomunicações, University of Aveiro, 3810-193 Aveiro, Portugal (e-mail: jcpedro@ua.pt).

Color versions of one or more of the figures in this paper are available online at http://ieeexplore.ieee.org.

Digital Object Identifier 10.1109/TMTT.2010.2095035

an important advantage of multitime ETHB over conventional ETHB is that it does not suffer from bandwidth restrictions [9] (one of the main limitations of conventional ETHB).

As we will see in the following sections, because we will treat the aperiodic slowly varying state variables only in the time domain, the proposed method can be seen as a hybrid scheme combining multitime ETHB [9]–[11] with a purely time-marching engine (SPICE-like simulation) for the baseband blocks.

II. Theoretical Background

A. Univariate and Multivariate Formulations

The behavior of an electronic circuit can be described with a system of differential algebraic equations in time, involving voltages, currents, charges, and fluxes. This system of equations can be constructed from a circuit description using, for example, nodal analysis, which involves applying the Kirchoff current law to each node in the circuit, and applying the constitutive or branch equations to each circuit element. Under the quasi-static assumption, [12], [13], systems generated this way have, in general, the following form:

$$\boldsymbol{p}[\boldsymbol{y}(t)] + \frac{d\boldsymbol{q}[\boldsymbol{y}(t)]}{dt} = \boldsymbol{x}(t) \tag{1}$$

where $\boldsymbol{x}(t) \in \mathbb{R}^n$ and $\boldsymbol{y}(t) \in \mathbb{R}^n$ stand for the excitation (independent voltage and current sources) and state variable (node voltages and branch currents) vectors, respectively. $\boldsymbol{p}[\boldsymbol{y}(t)]$ stands for all memoryless linear or nonlinear elements, such as resistors, or nonlinear controlled sources, while $\boldsymbol{q}[\boldsymbol{y}(t)]$ models dynamic linear or nonlinear elements, such as capacitors (represented as linear or nonlinear voltage-dependent electric charges) or inductors (represented as linear or nonlinear current-dependent magnetic fluxes).

When the circuit contains signals that evolve according to two widely separated time scales, as is the case of our illustrative application examples presented in Section IV, in which we have an aperiodic slow envelope time scale and a periodic fast carrier time scale, the numerical solution of (1) can be computed in a much more efficient way if multiple time variables are used to describe the multirate behavior [10], [11]. This strategy, commonly referred to as multivariate formulation, is based on the fact that multirate signals can be represented much more efficiently if they are defined as functions of two or more time variables, i.e., if they are defined as multivariate functions. With this multivariate formulation, circuits will be no longer described by ordinary differential algebraic equations in the univariate time t, but instead, by partial differential algebraic systems. In this study, we will adopt the following procedure: for the slowly varying parts (envelope time scale) of the expressions of $\boldsymbol{x}(t)$ and $\boldsymbol{y}(t)$, t is replaced by t_1; for the fast-varying parts (RF carrier time scale) t is replaced by t_2. The application of this bivariate strategy to the system of (1) converts it into the following multirate partial differential algebraic equations' system [10], [11]:

$$\boldsymbol{p}[\hat{\boldsymbol{y}}(t_1,t_2)] + \frac{\partial \boldsymbol{q}[\hat{\boldsymbol{y}}(t_1,t_2)]}{\partial t_1} + \frac{\partial \boldsymbol{q}[\hat{\boldsymbol{y}}(t_1,t_2)]}{\partial t_2} = \hat{\boldsymbol{x}}(t_1,t_2). \tag{2}$$

The mathematical relation between (1) and (2) establishes that, if $\hat{\boldsymbol{x}}(t_1,t_2)$ and $\hat{\boldsymbol{y}}(t_1,t_2)$ satisfy (2), then the univariate forms $\boldsymbol{x}(t) = \hat{\boldsymbol{x}}(t,t)$ and $\boldsymbol{y}(t) = \hat{\boldsymbol{y}}(t,t)$ satisfy (1) [10], [11]. Therefore, physically meaningful univariate solutions of (1) are available on diagonal lines $t_1 = t, t_2 = t$, along the bivariate solutions of (2), i.e., $\boldsymbol{y}(t)$ may be retrieved from its bivariate form $\hat{\boldsymbol{y}}(t_1,t_2)$ by simply setting $t_1 = t_2 = t$. Consequently, if one wants to obtain the univariate solution in some $[0, t_{\mathrm{Final}}]$ generic interval, due to the periodicity of the problem in t_2, we will have

$$\boldsymbol{y}(t) = \hat{\boldsymbol{y}}(t, t \bmod T_2) \tag{3}$$

on the rectangular domain $[0, t_{\mathrm{Final}}] \times [0, T_2]$, where T_2 is the period of the excitation and the solution in the t_2 dimension.

B. Multitime ETHB

Let us consider the bivariate formulation described by the multitime partial differential algebraic system of (2), together with the condition expressing the periodic regime in the t_2 dimension, $\hat{\boldsymbol{y}}(t_1,0) = \hat{\boldsymbol{y}}(t_1,T_2)$, characterizing the 2-D behavior of a nonlinear multirate RF circuit with n state variables, operating in an aperiodic slow time scale and a periodic fast carrier time scale. Let us also consider the semidiscretization of the rectangular domain $[0, t_{\mathrm{Final}}] \times [0, T_2]$ in the t_1 slow time dimension defined by

$$\begin{aligned} 0 = t_{1,0} < t_{1,1} < \cdots < t_{1,i-1} < t_{1,i} < \cdots < t_{1,N_1} \\ = t_{\mathrm{Final}}, \qquad h_{1,i} = t_{1,i} - t_{1,i-1}. \end{aligned} \tag{4}$$

If we use a finite-differences scheme (e.g., the backward Euler rule) to approximate the derivatives of (2) in t_1, we obtain, for each slow time instant $t_{1,i}$, a boundary value problem with periodic boundary conditions in the fast time t_2

$$\begin{aligned} \boldsymbol{p}[\hat{\boldsymbol{y}}_i(t_2)] + \frac{\boldsymbol{q}[\hat{\boldsymbol{y}}_i(t_2)] - \boldsymbol{q}[\hat{\boldsymbol{y}}_{i-1}(t_2)]}{h_{1,i}} \\ + \frac{d\boldsymbol{q}[\hat{\boldsymbol{y}}_i(t_2)]}{dt_2} = \hat{\boldsymbol{x}}_i(t_{1,i},t_2), \qquad \hat{\boldsymbol{y}}_i(0) = \hat{\boldsymbol{y}}_i(T_2). \end{aligned} \tag{5}$$

In order to obtain the whole solution $\hat{\boldsymbol{y}}(t_1,t_2)$ in the entire rectangular domain $[0, t_{\mathrm{Final}}] \times [0, T_2]$, a total of N_1 boundary value problems have to be solved. With multitime ETHB, the solution of each boundary value problem of (5) is evaluated by HB. The corresponding HB system for each slow time instant $t_{1,i}$ is the $n \times (2K+1)$ algebraic equations set given by

$$\begin{aligned} \mathbf{P}[\hat{\mathbf{Y}}(t_{1,i})] + \frac{\mathbf{Q}[\hat{\mathbf{Y}}(t_{1,i})] - \mathbf{Q}[\hat{\mathbf{Y}}(t_{1,i-1})]}{h_{1,i}} \\ + j\boldsymbol{\Omega}\mathbf{Q}[\hat{\mathbf{Y}}(t_{1,i})] = \hat{\mathbf{X}}(t_{1,i}) \end{aligned} \tag{6}$$

where $\hat{\mathbf{X}}(t_{1,i})$ and $\hat{\mathbf{Y}}(t_{1,i})$ are the vectors containing the Fourier coefficients of the excitation sources and of the solution (the state variables), respectively, at $t_1 = t_{1,i}$. $\mathbf{P}(\cdot)$ and $\mathbf{Q}(\cdot)$ are

unknown functions and $j\mathbf{\Omega}$ is the diagonal block matrix

$$j\mathbf{\Omega} = \mathrm{diag}\left(\underbrace{-jK\omega_0,\ldots,jK\omega_0}_{v=1},\underbrace{-jK\omega_0,\ldots,jK\omega_0}_{v=2},\ldots,\underbrace{-jK\omega_0,\ldots,jK\omega_0}_{v=n}\right) \quad (7)$$

with K being the order of the adopted harmonic truncation and $\omega_0 = 2\pi f_C$ (the carrier frequency). The $\hat{\mathbf{Y}}(t_{1,i})$ vector can be expressed as

$$\hat{\mathbf{Y}}(t_{1,i}) = [\hat{\mathbf{Y}}_1(t_{1,i})^T, \hat{\mathbf{Y}}_2(t_{1,i})^T, \ldots, \hat{\mathbf{Y}}_n(t_{1,i})^T]^T \quad (8)$$

where each one of the state variable frequency components, $\hat{\mathbf{Y}}_v(t_{1,i}), v = 1,\ldots,n$, is a $(2K+1)\times 1$ vector defined as

$$\hat{\mathbf{Y}}_v(t_{1,i}) = [Y_{v,-K}(t_{1,i}),\ldots,Y_{v,0}(t_{1,i}),\ldots,Y_{v,K}(t_{1,i})]^T. \quad (9)$$

Since $p(\cdot)$ and $q(\cdot)$ are, in general, nonlinear functions, one possible way to compute $\mathbf{P}(\cdot)$ and $\mathbf{Q}(\cdot)$ in (6) consists of evaluating $p(\cdot)$ and $q(\cdot)$ in the time domain and then calculate its Fourier coefficients. This way, the HB system of (6) can be rewritten as

$$\mathbf{F}[\hat{\mathbf{Y}}(t_{1,i})] = \mathbf{P}[\hat{\mathbf{Y}}(t_{1,i})] + \frac{\mathbf{Q}[\hat{\mathbf{Y}}(t_{1,i})] - \mathbf{Q}[\hat{\mathbf{Y}}(t_{1,i-1})]}{h_{1,i}} + j\mathbf{\Omega}\mathbf{Q}[\hat{\mathbf{Y}}(t_{1,i})] - \hat{\mathbf{X}}(t_{1,i}) = 0 \quad (10)$$

or, in its simplified form, as

$$\mathbf{F}[\hat{\mathbf{Y}}(t_{1,i})] = 0 \quad (11)$$

in which $\mathbf{F}[\hat{\mathbf{Y}}(t_{1,i})]$ is known as the error function at $t_1 = t_{1,i}$. In order to solve the nonlinear algebraic system of (11), a Newton–Raphson iterative solver is often used. In this case, the Newton–Raphson algorithm leads to

$$\mathbf{F}\left[\hat{\mathbf{Y}}^{[r]}(t_{1,i})\right] + \left.\frac{d\mathbf{F}[\hat{\mathbf{Y}}(t_{1,i})]}{d\hat{\mathbf{Y}}(t_{1,i})}\right|_{\hat{\mathbf{Y}}(t_{1,i})=\hat{\mathbf{Y}}^{[r]}(t_{1,i})} \times\left[\hat{\mathbf{Y}}^{[r+1]}(t_{1,i}) - \hat{\mathbf{Y}}^{[r]}(t_{1,i})\right] = 0 \quad (12)$$

which means that, at each iteration r, we have to solve a linear system of $n\times(2K+1)$ equations to compute the new estimate $\hat{\mathbf{Y}}^{[r+1]}(t_{1,i})$. Consecutive Newton iterations will be computed until a desired accuracy is achieved, i.e., until $\|\mathbf{F}[\hat{\mathbf{Y}}(t_{1,i})]\| < \mathrm{tol}$, where tol is the allowed error ceiling.

III. Innovative Simulation Method

A. Time-Domain Latency Within the Multivariate Formulation

In order to provide clarity in the explanation of the method proposed in this paper, let us start by considering a typical wireless system composed of baseband and RF blocks. If this system is to be simulated, at the circuit level, as a whole, it will show state variables (node voltages and currents), in the RF part, that are fast carrier envelope-modulated waveforms, and some others, typically in the baseband blocks, that are slowly varying aperiodic baseband signals. For concreteness, let us suppose that the signals

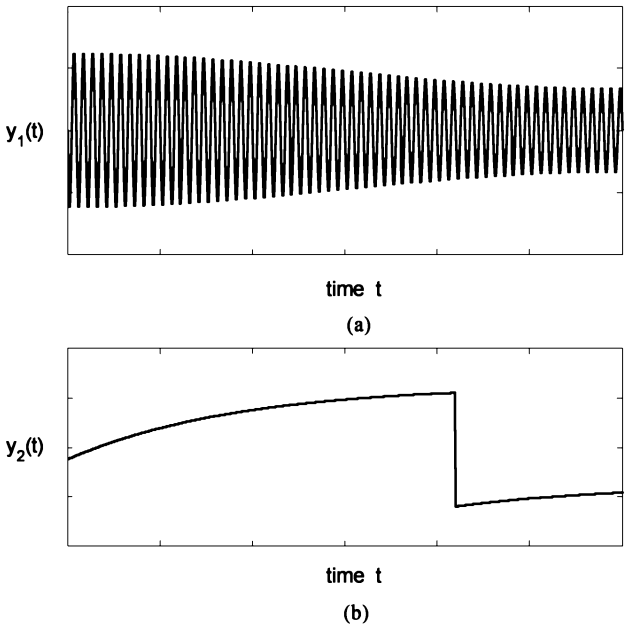

Fig. 1. Two distinct state variables. (a) Fast carrier envelope modulated waveform, $y_1(t)$. (b) Slowly varying aperiodic baseband signal, $y_2(t)$ with a sharp transition [5].

$$\begin{aligned} y_1(t) &= \sum_{k=-K}^{K} Y_k(t)e^{jk2\pi f_C t} \\ y_2(t) &= e(t) \end{aligned} \quad (13)$$

depicted in Fig. 1(a) and (b), are two distinct state variables in different parts of the circuit. $Y_k(t)$ represents the Fourier coefficients of $y_1(t)$, which are slowly varying in the baseband time scale, f_C is the carrier frequency, and $e(t)$ is a slowly varying aperiodic baseband function. In this paper, we will denote signals of the form of $y_1(t)$ as *active* and signals of the form of $y_2(t)$ as *latent*. The latency (slowness) revealed by $y_2(t)$ indicates that this variable belongs to a circuit block where there are no fluctuations dictated by the fast carrier. Consequently, it can be efficiently represented with much less sample points than $y_1(t)$. On the other hand, since it does not evidence any periodicity, it cannot be processed with HB [12]–[14]. Furthermore, if the number of harmonics K is not too large, the fast carrier oscillation components of $y_1(t)$ can be efficiently computed in the frequency domain. Consequently, since we are confronted with signals having completely different characteristics within the same problem, it is easy to conclude that distinct numerical strategies will be probably required for the evaluation of $y_1(t)$ and $y_2(t)$ if we want to simulate circuits having such signal format disparities in an efficient way.

In view of the fact that multitime ETHB operates in a bi-dimensional framework, let us now consider the bivariate forms

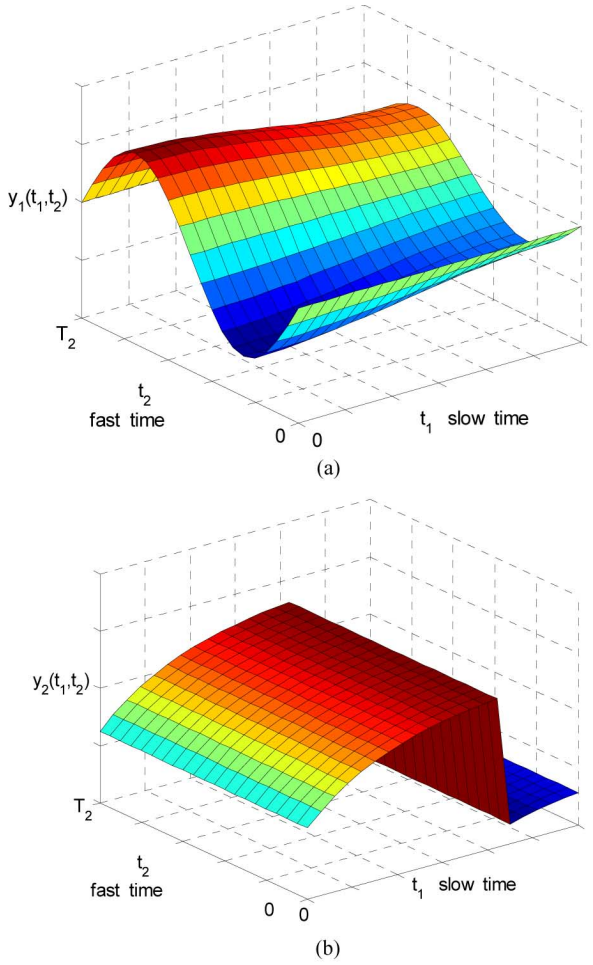

Fig. 2. Bivariate forms of the state variables shown in Fig. 1. (a) $\hat{y}_1(t_1, t_2)$. (b) $\hat{y}_2(t_1, t_2)$.

of $y_1(t)$ and $y_2(t)$, denoted by $\hat{y}_1(t_1, t_2)$ and $\hat{y}_2(t_1, t_2)$, and defined as

$$\begin{aligned}\hat{y}_1(t_1, t_2) &= \sum_{k=-K}^{K} Y_k(t_1) e^{jk2\pi f_C t_2} \\ \hat{y}_2(t_1, t_2) &= e(t_1)\end{aligned} \tag{14}$$

where t_1 and t_2 are, respectively, the slow envelope time dimension and the fast carrier time dimension. Fig. 2(a) and (b) depicts the plots of these bivariate entities on the $[0, t_{\text{Final}}] \times [0, T_2]$ rectangular domain, where $T_2 = 1/f_C$ is the carrier period. As is shown, $\hat{y}_2(t_1, t_2)$ has no fluctuations in the t_2 fast time axis because $y_2(t)$ does not oscillate at the carrier frequency. Consequently, for each slow time instant $t_{1,i}$ defined on the grid of (4), while $\hat{y}_1(t_{1,i}, t_2)$ is a waveform that has to be represented by a certain quantity $k = -K, \ldots, K$ of harmonic components, $\hat{y}_2(t_{1,i}, t_2)$ is merely a constant (dc) signal that can be simply represented by the $k = 0$ dc component.

B. Hybrid Time-Frequency Scheme

The system of (12) is typically a sparse linear system and several methods can be used to solve it, such as direct solvers, sparse solvers, or iterative solvers, but for very large systems, iterative solvers are usually preferred, and there is a general consensus that the generalized minimal residual (GMRES) [15] iterative technique is the preferred one for HB analysis [16]. The system of (12) involves the derivative of the vector $\mathbf{F}[\hat{\mathbf{Y}}(t_{1,i})]$ with respect to the vector $\hat{\mathbf{Y}}(t_{1,i})$. The result is a matrix, the so-called Jacobian of $\mathbf{F}[\hat{\mathbf{Y}}(t_{1,i})]$,

$$\begin{aligned}&\mathbf{J}[\hat{\mathbf{Y}}(t_{1,i})] \\ &\quad = \frac{d\mathbf{F}[\hat{\mathbf{Y}}(t_{1,i})]}{d\hat{\mathbf{Y}}(t_{1,i})} \\ &\quad = \begin{bmatrix} \frac{d\mathbf{F}_1[\hat{\mathbf{Y}}(t_{1,i})]}{d\hat{\mathbf{Y}}_1(t_{1,i})} & \frac{d\mathbf{F}_1[\hat{\mathbf{Y}}(t_{1,i})]}{d\hat{\mathbf{Y}}_2(t_{1,i})} & \cdots & \frac{d\mathbf{F}_1[\hat{\mathbf{Y}}(t_{1,i})]}{d\hat{\mathbf{Y}}_n(t_{1,i})} \\ \frac{d\mathbf{F}_2[\hat{\mathbf{Y}}(t_{1,i})]}{d\hat{\mathbf{Y}}_1(t_{1,i})} & \frac{d\mathbf{F}_2[\hat{\mathbf{Y}}(t_{1,i})]}{d\hat{\mathbf{Y}}_2(t_{1,i})} & \cdots & \frac{d\mathbf{F}_2[\hat{\mathbf{Y}}(t_{1,i})]}{d\hat{\mathbf{Y}}_n(t_{1,i})} \\ \cdots & \cdots & \cdots & \cdots \\ \frac{d\mathbf{F}_n[\hat{\mathbf{Y}}(t_{1,i})]}{d\hat{\mathbf{Y}}_1(t_{1,i})} & \frac{d\mathbf{F}_n[\hat{\mathbf{Y}}(t_{1,i})]}{d\hat{\mathbf{Y}}_2(t_{1,i})} & \cdots & \frac{d\mathbf{F}_n[\hat{\mathbf{Y}}(t_{1,i})]}{d\hat{\mathbf{Y}}_n(t_{1,i})} \end{bmatrix}\end{aligned} \tag{15}$$

which has a block structure consisting of a $n \times n$ matrix of square submatrices (blocks), each one with dimension $(2K + 1)$. Each block contains information about the harmonic components corresponding to the sensitivity of changes in a Fourier component of the error function $\mathbf{F}[\hat{\mathbf{Y}}(t_{1,i})]$, resulting from changes in any other component of that specific state variable. The general block of row m and column l can be expressed as

$$\begin{aligned}\frac{d\mathbf{F}_m[\hat{\mathbf{Y}}(t_{1,i})]}{d\hat{\mathbf{Y}}_l(t_{1,i})} = \frac{d\mathbf{P}_m[\hat{\mathbf{Y}}(t_{1,i})]}{d\hat{\mathbf{Y}}_l(t_{1,i})} + \frac{1}{h_{1.i}} \frac{d\mathbf{Q}_m[\hat{\mathbf{Y}}(t_{1,i})]}{d\hat{\mathbf{Y}}_l(t_{1,i})} \\ + j\Omega \frac{d\mathbf{Q}_m[\hat{\mathbf{Y}}(t_{1,i})]}{d\hat{\mathbf{Y}}_l(t_{1,i})}\end{aligned} \tag{16}$$

where $j\Omega = \text{diag}(-jK\omega_0, \ldots, 0, \ldots, jK\omega_0)$ is a diagonal matrix. $d\mathbf{P}_m[\hat{\mathbf{Y}}(t_{1,i})]/d\hat{\mathbf{Y}}_l(t_{1,i})$ and $d\mathbf{Q}_m[\hat{\mathbf{Y}}(t_{1,i})]/d\hat{\mathbf{Y}}_l(t_{1,i})$ denote, respectively, the conversion matrices (Toeplitz) of the vectors containing the Fourier coefficients of $dp_m[\hat{y}(t_{1,i}, t_2)]/d\hat{y}_l(t_{1,i}, t_2)$ and $dq_m[\hat{y}(t_{1,i}, t_2)]/d\hat{y}_l(t_{1,i}, t_2)$.

As illustrated above, bivariate forms of latent state variables have no undulations in the t_2 fast time scale. Hence, for each slow time instant $t_{1,i}$, they are merely constant (dc) node voltages or branch currents, which indicates that they can be completely represented by the corresponding $k = 0$ order Fourier coefficients. Thus, while active state variables have to be represented by a set of $(2K + 1)$ harmonic components arranged in vectors of the form of (9), latent state variables can be represented as scalar quantities, i.e.,

$$\hat{\mathbf{Y}}_v(t_{1,i}) = Y_{v,0}(t_{1,i}) = \hat{y}_v(t_{1,i}). \tag{17}$$

Taking this into account, it is easy to conclude that the size of the $\hat{\mathbf{Y}}(t_{1,i})$ vector defined by (8) can be considerably reduced, as also the total number of equations in the HB system of (10). An additional and important detail is that there is no longer any need to perform the conversion between time and frequency domains for the latent state variables expressed in the form of (17), as well as for the components of $\mathbf{F}[\hat{\mathbf{Y}}(t_{1,i})]$ corresponding to latent blocks of the circuit. Since the $k = 0$ order Fourier coefficient $Y_{v,0}(t_{1,i})$ is exactly the same as the constant t_2 time value $\hat{y}_v(t_{1,i})$, the use of the discrete Fourier transform (DFT) and the inverse discrete Fourier transform (IDFT)—or their fast algorithms, i.e., the fast Fourier transform (FFT) and the inverse

fast Fourier transform (IFFT)—will only be required for components in the HB system of (10) having dependence on active state variables. Thus, latent blocks are processed in a purely time-domain scheme as in any other time-marching simulation engine such as SPICE.

In what the Jacobian matrix (15) is concerned, significant matrix size reductions will also be achieved. Indeed, by taking into consideration this multirate characteristic (the subset circuit latency), some of the blocks of (15) will be merely 1×1 scalar elements, that contain dc information on the sensitivity of changes in components of $\mathbf{F}[\hat{\mathbf{Y}}(t_{1,i})]$ resulting from changes in latent components of $\hat{\mathbf{Y}}(t_{1,i})$. For instance, if the mth component of (15) is exclusively dependent on latent state variables and $\hat{y}_l(t_{1,i})$ is, itself, a latent state variable, then the block of row m and column l will simply be given by

$$\frac{d\mathbf{F}_m[\hat{\mathbf{Y}}(t_{1,i})]}{d\hat{\mathbf{Y}}_l(t_{1,i})} = \frac{dp_m[\hat{y}(t_{1,i})]}{d\hat{y}_l(t_{1,i})} + \frac{1}{h_{1,i}} \frac{dq_m[\hat{y}(t_{1,i})]}{d\hat{y}_l(t_{1,i})}. \quad (18)$$

The 1×1 (scalar) Jacobian matrix block of (18) can be viewed as a special case of the general $(2K+1) \times (2K+1)$ block of (16) if we assume $K = 0$ as the maximum harmonic order. In fact, since $df_m[\hat{y}(t_{1,i}, t_2)]/d\hat{y}_l(t_{1,i}, t_2)$ is a basic constant function presenting no fluctuations in the t_2 fast time scale, there will be no necessity to convert the right-hand side terms of (18) into the frequency domain. In addition, the third term of (16) is zero, thus being simply discarded.

From the above considerations, we expect that significant computation and memory savings may be achieved when finding the solution of (10). Indeed, with the state variable $\hat{\mathbf{Y}}(t_{1,i})$ and the error function $\mathbf{F}[\hat{\mathbf{Y}}(t_{1,i})]$ vector size reductions, as also the resulting Jacobian $\mathbf{J}[\hat{\mathbf{Y}}(t_{1,i})]$ matrix size reduction, we can avoid dealing with large linear systems in the iterations of (12). Thus, a less computationally expensive Newton-Raphson iterative solver will be required.

An important note in this respect should refer that this advantage is increasingly evident as the ratio of the number of latent to the number of active state variables rises, which corresponds to the trend we today face in modern RFICs or SoC for mass-production wireless applications.

C. Bivariate and Univariate Grids

A final remark that refers to the disparity between active and latent blocks of a circuit regards the number of time samples used for representing the corresponding state variables. As suggested above, the number of sample points required for the active and latent parts will be obviously different. In fact, according to the adopted harmonic truncation, at least $(2K+1)$ sample points per slow time instant $t_{1,i}$ will be needed for computing the active state variables' waveforms in the t_2 dimension. In contrast, only one time sample will be required for representing the latent state variables at each time instant $t_{1,i}$. Thus, what we are actually doing with this newly proposed method is to process the active state variables with a bi-dimensional mixed time-frequency domain scheme—where the envelope is processed in the t_1 slow time scale, while the steady-state response to the carrier is processed in the frequency-domain—and the latent state variables with a purely 1-D time-domain engine. That is, bivariate forms of the active state variables are discretized in both the t_1 and t_2 dimensions of the $[0, t_{\mathrm{Final}}] \times [0, T_2]$ rectangular domain, according to (4), and to the following uniform grid:

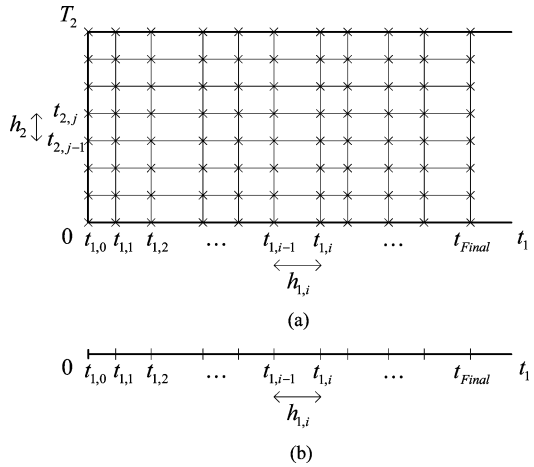

Fig. 3. Bivariate and univariate grids for the evaluation of: (a) active state variables and (b) latent state variables.

$$0 = t_{2,0} < t_{2,1} < \cdots < t_{2,j-1} < t_{2,j} < \cdots < t_{2,N_2} = T_2$$
$$h_2 = t_{2,j} - t_{2,j-1} = T_2/N_2 \quad (19)$$

where $N_2 \geq 2K+1$ is the total number of sample points used per slow time instant $t_{1,i}$. Conversely, latent state variables are treated as purely univariate t_1 slow time-dependent entities, being evaluated only on the 1-D grid defined by (4). This is illustrated in Fig. 3(a) and (b).

D. Circuit Partitioning Strategy

In order to put into practice a mixed time-frequency simulator capable to benefit from the multirate approach presented above, a partitioning strategy allowing automatic classification of the circuit's state variables (as active or latent) must be included in the simulation package. Therefore, we will now present a circuit partitioning strategy with two distinct variants, which will split the circuit into active and latent sub-circuits, according to the time rates of change of its state variables. The former is conceived for RF circuits with dynamic subset division (circuits in which the partition into active and latent sub-circuits may vary with time), and the later is tailored for RF circuits with static subset division (circuits in which the partition does not change along the simulation process). These strategy variants are described in detail in the following.

For a general RF circuit with dynamic active-latent partition, we iteratively solve the periodic boundary value problem of (5) at each slow time instant $t_{1,i}$ using the multitime ETHB engine on the first iteration of (12), and the newly proposed hybrid scheme on the subsequent iterations. With this methodology, we start by considering all the circuit's state variables as active, that is, we start by representing all the state variables in the frequency domain as a set of $(2K+1)$ harmonic components. Thus, to obtain the solution of (10), a single Newton iteration (12) is carried out to achieve $\hat{\mathbf{Y}}^{[1]}(t_{1,i})$. Each one of its

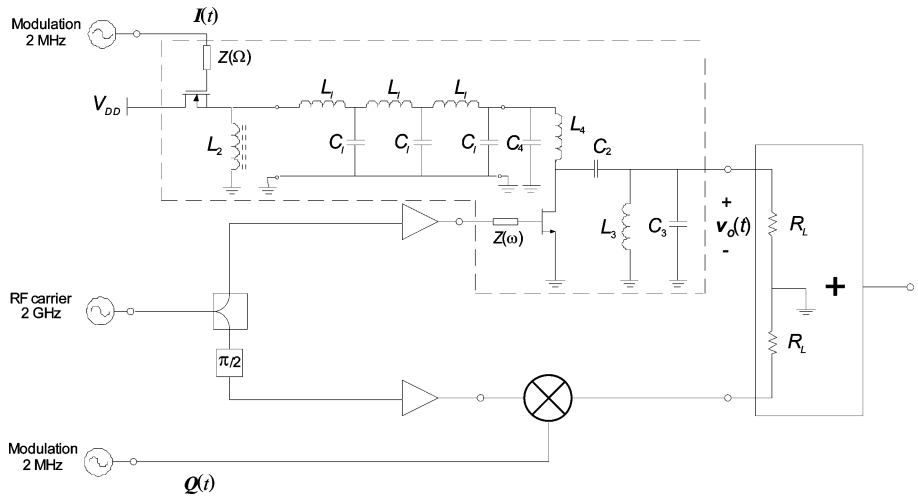

Fig. 4. Low-distortion I/Q modulator, showing the simplified schematic of the single section actually simulated.

state variable Fourier coefficients vector, $\hat{\mathbf{Y}}_v^{[1]}(t_{1,i})$, is then examined. With the exception of the $k = 0$ order (dc component), state variables whose Fourier coefficients' absolute values stay under a very small prescribed tolerance will be classified as latent. The remaining state variables will be classified as active. After this state variable classification, which will temporarily divide the circuit into active and latent sub-circuits, we automatically switch to the hybrid scheme (benefiting from all the advantages described above) to perform the subsequent numerical iterations that will conduct to the solution of (5).

We would like to point out that more than one iteration with the multitime ETHB engine may be required before switching to the new hybrid technique. This will increase the robustness of the above partitioning strategy. However, it obviously will conduct to some efficiency reduction of the method. We may also note that the state variable classification described above could also be defined in the time domain. For instance, when we perform inverse Fourier transformation of $\hat{\mathbf{Y}}^{[1]}(t_{1,i})$, to get its time-domain equivalent, $\hat{y}^{[1]}(t_{1,i}, t_2)$, the latent state variables will be those that practically evidence no fluctuations in the fast time t_2.

Since many RF circuits have a static subset partition (as is the case of our RF sample applications presented in Section IV), it will be helpful if we can profit from this feature. That is, a more suitable circuit partitioning strategy than the one presented above will certainly reduce the computational effort. In this case, we have decided to proceed as follows. We start by computing the solution of the periodic boundary value problem of (5) for the first slow time instant $t_{1,1}$ exclusively using the multitime ETHB engine. We then split the circuit into active and latent sub-circuits, according to the fluctuations of the state variables $\hat{y}_v(t_{1,1}, t_2)$ in the t_2 fast time scale. Those which do not evidence oscillations in t_2 will be classified as latent. The remaining ones will be classified as active. This classification provides a permanent active-latent sub-circuit division, and it is based on it we will proceed computing the solution of the problem for the remaining $t_{1,i} = t_{1,2}, \ldots, t_{1,N_1}$ slow time instants with the newly proposed time-frequency hybrid technique.

IV. Illustrative Application Examples

We will now test the performance and the efficiency of the newly proposed method through its application to two simple illustrative examples, which are: 1) a low distortion I/Q modulator and 2) an RF polar transmitter schematic with a hybrid envelope amplifier. Circuits with distinct configurations and levels of complexity were especially selected to illustrate how the computational efficiency of the proposed method is made more and more evident as the ratio between the number of latent and active state variables is increased.

A. Low Distortion I/Q Modulator

The nonlinear circuit of Fig. 4 depicts a simplified schematic of a single section of a low-distortion in-phase/quadrature (I/Q) modulator to be used in a Cartesian transmitter.

This circuit, based on a highly linear resistive FET modulator, includes two independent excitations of very separated time scales: the baseband input signal, whose bandwidth is around 2 MHz, and the RF carrier of $f_C = 2$ GHz. Beyond the simultaneous presence of periodic (RF carrier) and aperiodic (baseband input signal) forcing functions of very distinct time scales, in this nonlinear circuit, we also have a combination of heterogeneous state variables of widely disparate rates of variation. For instance, while voltages and currents in the RF MOSFET are very fast, voltages and currents in the baseband MOSFET are much slower. Thus, the former are classified as active state variables, while the later are considered latent state variables. In this particular circuit example, the ratio of the number of latent to active state variables is 2.

The resistive FET modulator of Fig. 4 was simulated in MATLAB with the newly proposed method versus the ETHB technique. Since ETHB is a well-known computer-aided design (CAD) tool in the RF and microwave community, the results obtained with this recognized technique are used as a reference for measuring both the computational speed and the accuracy of the new method. In our experiments, a dynamic step size control tool was used in the t_1 slow time scale, and we considered $K = 9$ as the maximum harmonic order for the HB

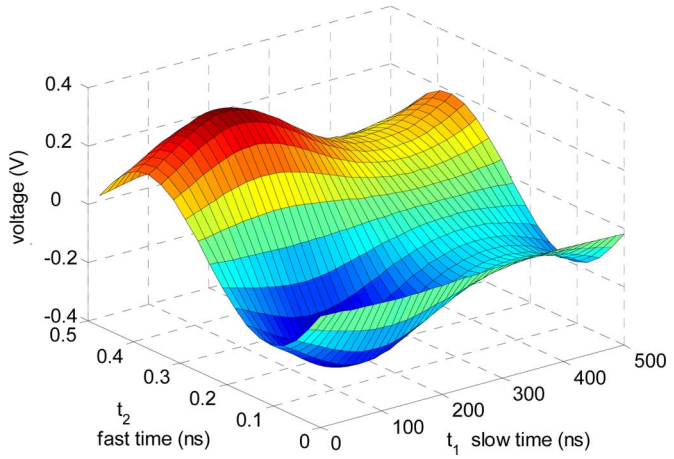

Fig. 5. Bivariate output voltage $v_O(t_1, t_2)$ obtained from the circuit of Fig. 4. Note the dependence of $v_O(t_1, t_2)$ on the slowly varying envelope time scale t_1 and the fast varying time scale t_2.

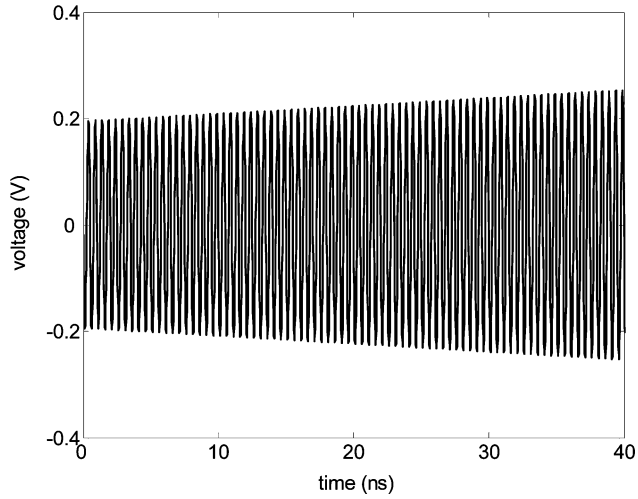

Fig. 6. Univariate representation of the output voltage $v_O(t)$ corresponding to the bivariate version of the state variable depicted in Fig. 5.

evaluations ($2K + 1 = 19$ sample points were used in the t_2 fast time scale).

Fig. 5 shows the bivariate solution of the output voltage of the circuit, on the $[0, 0.5\ \mu\text{s}] \times [0, 0.5\ \text{ns}]$ rectangular domain, while its corresponding univariate version—recovered from the multivariate form setting $y_v(t) = \hat{y}_v(t, t \bmod T_2)$—is depicted in Fig. 6, for the $[0, 40\ \text{ns}]$ time interval. This is an example of a fast-varying (active) state variable, which is the reason why it was computed in the bi-dimensional t_1, t_2 framework.

Fig. 7 depicts the univariate solution in the $[0, 0.5\ \mu\text{s}]$ time interval, for the L_2 inductor current. As this current is a latent state variable, it was computed in a purely 1-D time approach.

Numerical computation times (in seconds) and errors in the output voltage of the circuit are presented in Table I for simulations in the $[0, 0.5\ \mu\text{s}]$ and $[0, 5.0\ \mu\text{s}]$ intervals. As can be seen, efficiency gains of about six times were achieved with the new method, without compromising the accuracy of the results. Indeed, the discrepancy between the solutions obtained with the new method and with the standard ETHB, for all the other state variables of the circuit, is on the same order of magnitude of the

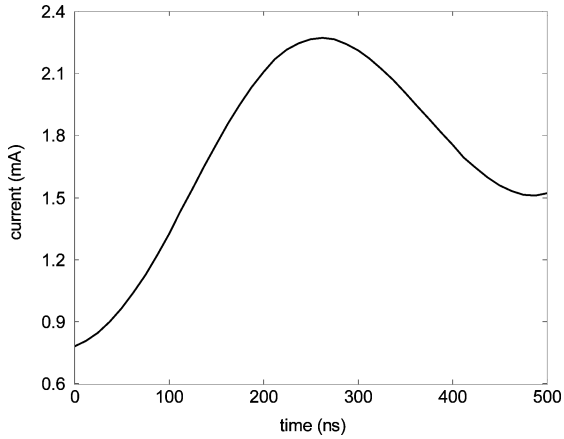

Fig. 7. Univariate L_2 inductor current of the circuit of Fig. 4.

TABLE I
NUMERICAL SIMULATION RESULTS FET MODULATOR

Simulation time interval	Computation time (s) Newly proposed method	Computation time (s) ETHB	Speedup approx.	Error in v_O Max. error (V)	Error in v_O Mean squared error (V^2)
[0, 0.5 μs]	2.1	12.8	6.1	4.66×10^{-8}	3.73×10^{-16}
[0, 5.0 μs]	19.8	126.4	6.4	4.66×10^{-8}	3.28×10^{-16}

one presented in Table I for the output voltage (mean squared errors of the order of 10^{-16}).

B. RF Polar Transmitter With a Hybrid Envelope Amplifier

The second example we used to test the capabilities of the newly proposed method is the nonlinear circuit of Fig. 8 [5], which is a simplified RF polar transmitter schematic with a hybrid (linear plus switching mode) envelope amplifier [17], [18]. As described in [5], this circuit includes three independent excitations running in two widely separated time scales: the magnitude $\text{AM}(t)$ and phase $\text{PM}(t)$ baseband input signals, whose bandwidth is around 200 kHz, and the RF carrier of $f_C = 2$ GHz frequency. It presents also a combination of heterogeneous state variables with widely disparate rates of variation (active and latent state variables), and the ratio of the number of latent to active state variables is now 4.5. For instance, voltages and currents in the RF MOSFET and in the output bandpass filter are all very fast, i.e., they oscillate at a rate dictated by the RF carrier, and thus will be detected as active state variables. Conversely, voltages and currents in the AM linear stage, in the current sense comparator, or even in the switch stage, are all much slower, and thus will be detected as latent state variables. This means that the switching behavior of the current sense comparator and of the devices included in the switch stage will be processed with a purely time-domain approach, while the smooth nonlinearities of the RF part will be treated in the frequency domain.

The circuit of Fig. 8 was simulated in MATLAB with the newly proposed method and with the standard ETHB technique. Once again, the numerical results obtained with ETHB are used as a reference for assessing both the computational speed and the

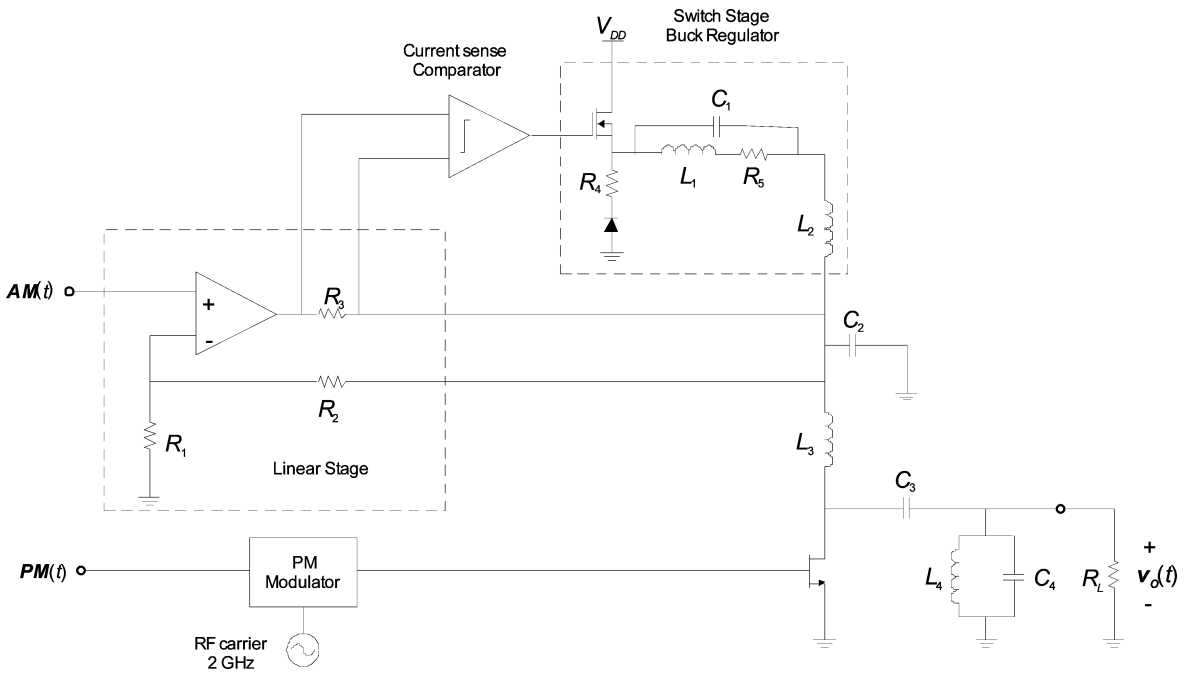

Fig. 8. RF polar transmitter with a hybrid envelope amplifier [5].

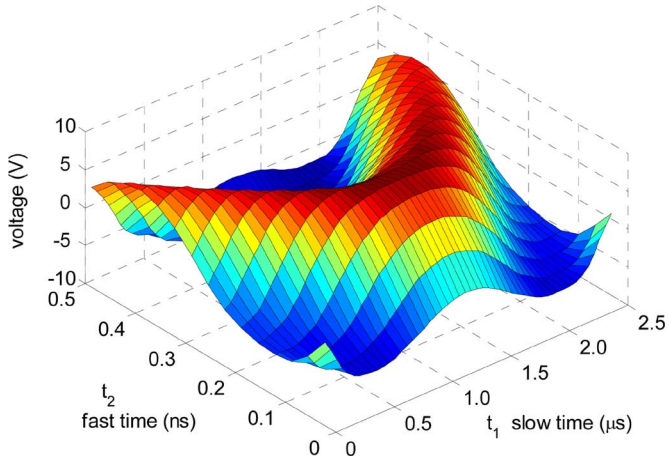

Fig. 9. Bivariate output voltage $v_O(t_1, t_2)$ obtained from the circuit of Fig. 8. Note the dependence of $v_O(t_1, t_2)$ on the slowly varying envelope time scale t_1 and the fast varying time scale t_2.

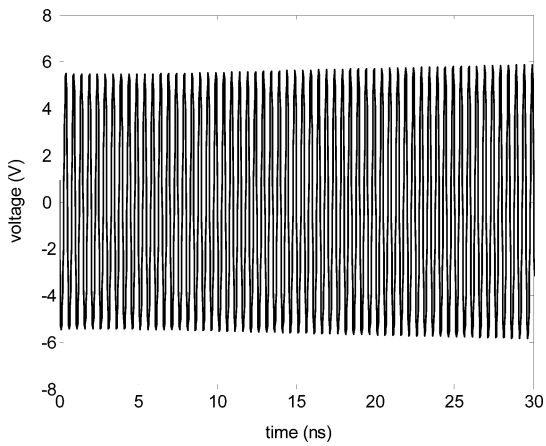

Fig. 10. Univariate representation of the output voltage $v_O(t)$ corresponding to the bivariate version of the state variable depicted in Fig. 9.

accuracy of the new method. In the same way as in the FET modulator, a dynamic step size control tool was used in the t_1 slow time scale, and we considered $K = 9$ as the maximum harmonic order for the HB evaluations.

Fig. 9 shows the bivariate solution of the circuit's output voltage, on the $[0, 2.5\ \mu\text{s}] \times [0, 0.5\ \text{ns}]$ rectangular domain. This is an example of a fast-varying (active) state variable in the circuit, reason why it was computed in the bi-dimensional t_1, t_2 framework. The plot of the univariate version of this state variable, recovered from its corresponding multivariate form by setting $y_v(t) = \hat{y}_v(t, t \bmod T_2)$, is depicted in Fig. 10 for the $[0, 30\ \text{ns}]$ time interval.

Figs. 11–13 depict the solutions in the $[0, 2.5\ \mu\text{s}]$ time interval, for the switch stage MOSFET source voltage, the L_1 inductor current and the C_2 capacitor voltage (the dynamic RF power transistor drain voltage supply), respectively. These are all slowly varying (latent) state variables, and thus they were represented with a purely 1-D time-domain scheme.

Numerical computation times (in seconds) and errors in the output voltage of the circuit, for simulations in the $[0, 1.0\ \mu\text{s}]$ and $[0, 5.0\ \mu\text{s}]$ intervals are presented in Table II. As we can see, speedups of more than one order of magnitude were now obtained for the simulation of this illustrative example. Once again, the accuracy of the results obtained with the proposed method, as compared to the standard ETHB, is very good, with mean squared errors on the order of 10^{-17} for v_O, and of similar order of magnitude for all the other circuit's state variables.

Tables I and II attest an expected significant speedup gain of about 6–19, a direct consequence of the increased ratio of the number of latent to active state variables from 2 to 4.5 (in the

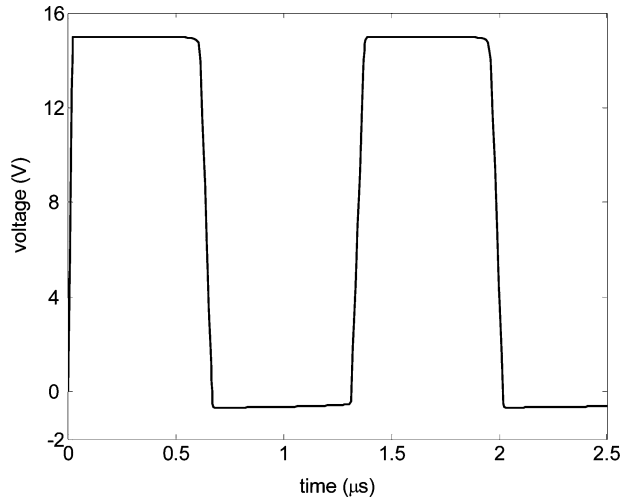

Fig. 11. Switch stage transistor source voltage (see Fig. 8).

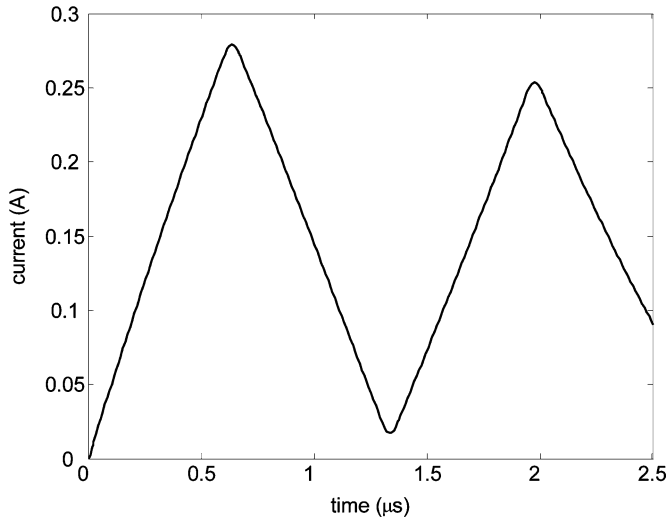

Fig. 12. L_1 inductor current of the circuit of Fig. 8.

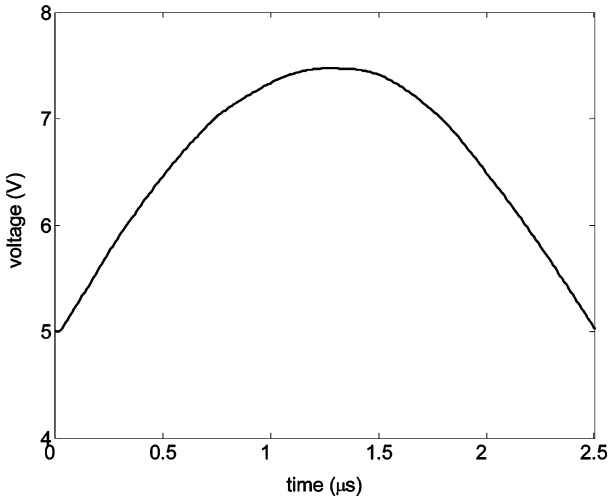

Fig. 13. C_2 capacitor voltage of the circuit of Fig. 8. This is the envelope modulated drain voltage supplied to the RF power transistor.

resistive FET modulator and the RF polar transmitter, respectively).

TABLE II
NUMERICAL SIMULATION RESULTS RF POLAR TRANSMITTER WITH HYBRID ENVELOPE AMPLIFIER

Simulation time interval	Computation time (s)		Speedup approx.	Error in v_O	
	Newly proposed method	ETHB		Max. error (V)	Mean squared error (V^2)
[0, 1.0 μs]	6.0	106.2	17.7	1.68×10^{-8}	6.85×10^{-17}
[0, 5.0 μs]	25.3	484.6	19.2	1.85×10^{-8}	4.80×10^{-17}

Several other simulations under different conditions (different initial conditions, diverse baseband signals, and diverse time intervals) were conducted for both examples, and the results in terms of speedup and accuracy were always similar to the ones presented in Tables I and II.

V. CONCLUSION

In this paper, we presented an innovative technique to simulate modern wireless systems, as a whole, at the circuit level. Recognizing that these systems are composed of a large set of low-frequency baseband circuits, plus some RF/microwave circuits, and that the former are more easily solved in the time domain, while the latter are more efficiently dealt with in the frequency domain, the proposed method uses a hybrid combination of time-marching and HB simulation engines.

From the numerical point of view, the proposed simulation method can be seen as a hybrid scheme that combines multitime ETHB based on the multivariate formulation, with a pure time-marching engine. In this way, fast changing, and modulated, RF (active) state variables are processed in a bivariate mixed time-frequency domain, whereas slowly varying baseband (latent) state variables are treated in the natural 1-D time domain.

By splitting the circuits into these two different parts, and taking advantage of the fact that there is no necessity to perform the conversion between time and frequency domains for the state variables in the latent part, significant computation speedups and memory savings were achieved without compromising accuracy. Although the achieved speedups are already quite impressive, it is worth noting that much higher values should be expected in real circuits. Indeed, as these speedups were shown to increase with the ratio of the number of latent to active state variables—in our simplified examples, these ratios were only 2 and 4.5 and already led to speedups of 6 and 19—one can get an idea of the potential of this time-frequency hybrid simulation technique when applied to real circuits where these ratios may be several orders of magnitude higher than the ones tested.

REFERENCES

[1] D. Sharrit, "New method of analysis of communication systems," presented at the IEEE MTT-S Nonlinear CAD Workshop, Jun. 1996.

[2] E. Ngoya and R. Larchevèque, "Envelope transient analysis: A new method for the transient and steady-state analysis of microwave communications circuits and systems," in *IEEE MTT-S Int. Microw. Symp. Dig.*, San Francisco, CA, Jun. 1996, pp. 1365–1368.

[3] V. Rizzoli, A. Neri, and F. Mastri, "A modulation-oriented piecewise harmonic balance technique suitable for transient analysis and digitally modulated analysis," in *Proc. 26th Eur. Microw. Conf.*, Prague, Czech Republic, Oct. 1996, pp. 546–550.
[4] D. Sharrit, "Method for simulating a circuit," U.S. Patent 5 588 142, Dec. 24, 1996.
[5] J. Oliveira and J. C. Pedro, "A new mixed time-frequency simulation method for nonlinear heterogeneous multirate RF circuits," in *IEEE MTT-S Int. Microw. Symp. Dig.*, Anaheim, CA, May 2010, pp. 548–551.
[6] H. Asai and H. Makino, "Frequency domain latency and relaxation-based harmonic analysis of nonlinear circuits," in *Proc. 34th Midwest Circuits Syst. Symp.*, Monterey, CA, May 1991, pp. 202–205.
[7] H. Makino and H. Asai, "Acceleration techniques for the circuit simulation in the frequency domain," in *Proc. IEEE Int. Circuits Syst. Symp.*, San Diego, CA, May 1992, pp. 903–906.
[8] V. Rizzoli *et al.*, "Domain-decomposition harmonic balance with block-wise constant spectrum," in *IEEE MTT-S Int. Microw. Symp. Dig.*, San Francisco, CA, Jun. 2006, pp. 860–863.
[9] J. C. Pedro and N. B. Carvalho, "Simulation of RF circuits driven by modulated signals without bandwidth constraints," in *IEEE MTT-S Int. Microw. Symp. Dig.*, Seattle, WA, Jun. 2002, pp. 2173–2176.
[10] J. Roychowdhury, "Efficient methods for simulating highly nonlinear multirate circuits," in *Proc. 34th Design Automat. Conf.*, Anaheim, CA, Jun. 1997, pp. 269–274.
[11] J. Roychowdhury, "Analyzing circuits with widely separated time scales using numerical PDE methods," *IEEE Trans. Circuits Syst. I, Fundam. Theory Appl.*, vol. 5, no. 48, pp. 578–594, May 2001.
[12] P. J. Rodrigues, *Computer-Aided Analysis of Nonlinear Microwave Circuits*. Norwood, MA: Artech House, 1998.
[13] S. A. Maas, *Nonlinear Microwave and RF Circuits*, 2nd ed. Norwood, MA: Artech House, 2003.
[14] K. Kundert, J. White, and A. Sangiovanni-Vincentelli, *Steady-State Methods for Simulating Analog and Microwave Circuits*. Norwell: Kluwer, 1990.
[15] Y. Saad and M. Schultz, "GMRES: A generalized minimal residual method for solving nonsymmetric linear systems," *SIAM J. Sci. Statist. Comput.*, vol. 7, pp. 856–869, Jul. 1986.
[16] V. Rizzoli, F. Mastri, C. Cecchetti, and F. Sgallari, "Fast and robust inexact Newton approach to the harmonic-balance analysis of nonlinear microwave circuits," *IEEE Microw. Guided Wave Lett.*, vol. 7, no. 10, pp. 359–361, Oct. 1997.
[17] P. Asbeck, L. Larson, D. Kimball, F. Wang, J. Jeong, P. Draxler, and C. Hsia, "Envelope elimination and restoration technology for high efficiency base station applications," presented at the IEEE MTT-S WMB High Efficiency Amplifiers Workshop, 2006.
[18] F. Wang *et al.*, "An improved power-added efficiency 19-dBm hybrid envelope elimination and restoration power amplifier for 802.11g WLAN applications," *IEEE Trans. Microw. Theory Tech.*, vol. 54, no. 12, pp. 4086–4099, Dec. 2006.

Jorge F. Oliveira was born in Leiria, Portugal, in 1965. He received the Diploma degree in electrical engineering (electronics and telecommunications) and Master of Science degree in applied mathematics from the University of Coimbra, Coimbra, Portugal, in 1989 and 2005, respectively, and the Doctoral degree in electrical engineering from the University of Aveiro, Aveiro, Portugal, in 2010.

He is currently a Professor with the Polytechnic Institute of Leiria, Leiria, Portugal. His current research interests include CAD techniques for nonlinear circuit analysis and system simulation.

José C. Pedro (S'90–M'95–SM'99–F'07) was born in Espinho, Portugal, on March 7, 1962. He received the Diploma, Doctoral, and Habilitation degrees in electronics and telecommunications engineering from the University of Aveiro, Aveiro, Portugal, in 1985, 1993 and 2002, respectively.

From 1985 to 1993, he was an Assistant Lecturer with the University of Aveiro, and since 1993, a Professor. He is currently also a Senior Research Scientist with the Instituto de Telecomunicações, Department of Electronics, Telecommunications, and Informatics, University of Aveiro. His main scientific interests include active device modeling and the analysis and design of various nonlinear microwave and opto-electronics circuits, in particular, the design of highly linear multicarrier power amplifiers and mixers. He is the lead author of *Intermodulation Distortion in Microwave and Wireless Circuits* (Artech House, 2003). He has authored or coauthored over 100 papers in international journals and symposia.

Dr. Pedro has served the IEEE in the Portuguese Microwave Theory and Techniques (MTT)/Antennas and Propagation (AP)/Electron Device (ED) Joint Chapter and the MTT-11 Technical Committee. He is a reviewer and associate editor for the IEEE TRANSACTIONS ON MICROWAVE THEORY AND TECHNIQUES. He is a reviewer for the IEEE Microwave Theory and Techniques Society (IEEE MTT-S) International Microwave Symposium (IMS). He was the recipient of the 1993 Marconi Young Scientist Award and the 2000 Institution of Electrical Engineers (IEE), U.K., Measurement Prize.